International Journal of Multidisciplinary Research and Growth Evaluation.

Effect of post-synthesis betanin functionalized silver nanoparticles on the cellular oxidative mechanism and biofilm formation in *Staphylococcus aureus*

Kenneth Munene Mbae [1*], Sri Raghava [2], Sharanaiah Umesha [3]
[1, 3] Department of Studies in Biotechnology, University of Mysore, Manasagangotri, Mysuru-570006, Karnataka, India
[2] Department of Biotechnology, Karnataka State Open University, Mukhtagangotri, Mysuru-570006, Karnataka, India
[1] Department of Food Science, Meru University of Science and Technology P.O. BOX 972, Meru 60200, Kenya

* Corresponding Author: **Kenneth Munene Mbae**

Article Info

ISSN (online): 2582-7138
Impact Factor: 5.307 (SJIF)
Volume: 04
Issue: 06
November-December 2023
Received: 21-08-2023;
Accepted: 23-09-2023
Page No: 219-228

Abstract
Eliciting oxidative stress and interference with biofilm formation by silver nanoparticles (AgNPs) comprise some of the postulated mechanisms of bacteria destruction. Plant extracts are commonly employed both as reducing agents and stabilizers of green-synthesized AgNPs. This yields a broad nanoparticle size distribution and unpredictable coating arising from diverse biomolecules and oxidation products in the final reaction mixture, which makes the comparison of different experiments exploiting green synthesised AgNPs as antimicrobial agents tricky. The current study synthesised citrate-capped silver nanoparticles (CtAgNPs) with a diameter of 37.9±8.6 nm functionalized via ligand exchange with betanin. Subsequently, the betanin silver nanoparticles (BtnAgNPs) ability to perturb the cellular oxidative stress defence mechanism of *Staphylococcus aureus* American Type Culture Collection (ATCC) 12600 and biofilm-forming properties were evaluated. Treatment with a minimum inhibitory concentration (MIC) of BtnAgNPs (12.5ppm) promoted reactive oxygen species accumulation and significantly reduced superoxide dismutase (SOD) and catalase activities. Furthermore, BtnAgNPs at sub-minimum inhibitory concentrations (SubMICs) to MIC range (0.39-12.5 ppm) inhibited the establishment of biofilms in a concentration-dependent manner. The study advocates for synthesis protocols that produce precise-sized nanoparticles followed by selective biomolecule functionalization for better antimicrobial efficacy comparative studies between AgNPs bearing different coatings in future experiments.

DOI: https://doi.org/10.54660/.IJMRGE.2023.4.6.219-228

Keywords: Silver nanoparticles, oxidative stress, reactive oxygen species, *Staphylococcus aureus*

1. Introduction

A nanotechnology-based approach using several types of metallic nanoparticles that have antimicrobial properties and other nano-dimension antibiotic carriers is gaining attention as a novel way of controlling pathogenic micro-organisms [1-3]. This provides a new arsenal against emerging pathogens that resist traditional antibiotics. The effectiveness of silver nanoparticles (AgNPs) as antimicrobial agents on diverse pathogens has been effectively demonstrated. Nevertheless, nanoparticles' precise destructive routes are an area of continuing investigation.

Dos Santos *et al*. [4] reviewed some plausible mechanisms proposed by researchers. Silver and other metallic nanoparticles hinder growth and diminish cell viability via multiple cellular pathways. One of the ways is the nanoparticles contacting the mitochondrial membrane, which activates genes linked to apoptosis and ultimately causes apoptosis [5]. Additionally, mitochondrial damage results in the production of reactive oxygen species (ROS), which degrade DNA [6]. Moreover, DNA is damaged via direct interaction with nanoparticles. Synthesis inhibition and oxidation of proteins following the attachment of nanoparticles to ribosomes have been suggested as possible mechanisms too.

Furthermore, the build-up of nanoparticles on the plasma membrane of the cell causes temporary or complete damage to the conformation and/or functionality of the surface proteins, which results in the formation of holes. This permits nanoparticles to enter the cell and cell components to leak [7]. Specifically, Bethyl *et al*. [8] proposed that AgNPs could induce cell death in *Escherichia coli* by the creation of "pits" on the cell wall, increasing membrane permeability and eventual respiratory chain inactivation. Conversely, the silver ions arising from the dissolution of AgNPs can bind to the thiol and amino groups on the cell wall occasioning disruption of protein structure [9].

Triggering oxidative stress imbalance by antimicrobial agents is postulated to lead to the destruction of bacteria [10, 11]. Strong evidence has been presented by studies demonstrating that AgNPs cause cell death in a variety of bacteria, including *S. aureus, Klebsiella pneumoniae E. coli, Bacillus subtilis, Helicobacter felis, Helicobacter pylori, Salmonella flexneri, Pseudomonas aeruginosa* and *Streptococcus pneumoniae*, through the formation of ROS [12, 13]. Quercetin-mediated AgNPs were effective against multi-drug resistant *P. aeruginosa* and *S. aureus* from goats with mastitis, at 1 and 2 ppm minimum inhibitory concentration (MIC) respectively. In the study, ROS generation and disruption of cell membrane integrity accompanied the nanoparticle's bactericidal activity [14].

S. aureus occurs ubiquitously on humans' and animals' skin, and mucous membranes. It is a remarkably versatile organism, well adapted to its human host. Normally this colonisation is asymptomatic and goes unnoticed. However, *S. aureus* is frequently involved in mucous membranes and skin infections. It can also turn on its host and trigger a range of infections, from minor skin and soft tissue infections to fatal sepsis [15]. Currently, *S. aureus* is a frequent isolate from patients. From a clinical perspective, hard-to-treat infections caused by methicillin-resistant *S. aureus* (MRSA) are a major concern. The World Health Organization (WHO) has highlighted the increasing occurrence of severe hospital and community infections associated with first-line drug-resistant *S. aureus*. It is estimated that individuals with MRSA are 64% more likely to succumb than those with non-resistant infections. Consequently, MRSA plus other subtypes of antibiotic-resistant microbes e.g. *E. coli* and *K. pneumoniae*, which cause nosocomial infections, and *Mycobacterium tuberculosis* causing multidrug-resistant tuberculosis, have been singled out as disease-causing organisms of global concern warranting special interest to ameliorate their threat [16].

On the other hand Park and Seo [17] noted that gastroenteritis from staphylococcal food poisoning (SFP) is very common globally. It is caused by ingesting food contaminated by *Staphylococcus* containing preformed staphylococcal enterotoxins. The toxins are heat resistant and can withstand 100 ℃ for 30 min. In the *Staphylococcus* genus, *S. aureus* has been singled as the predominant cause of SFP. The intoxication is characterized by abdominal cramps, vomiting and diarrhoea.

Initially, it was thought that MRSA was a human-associated problem and more so a hospital-acquired infection. However, MRSA has been encountered in pets, and farm animals used as food and their products, indicating its permeation into the food chain [18-20]. MRSA isolates from milk and their products have been found to produce enterotoxin [21]. Consequently, finding new and effective ways of controlling MRSA is a priority for medical and food microbiologists.

The existence of biofilms is a normal occurrence in nature among many microbial species. It helps microbes resist external stresses. Biofilm formation is a prominent virulence factor of *S. aureus* [22]. Silver nanoparticles have been demonstrated to inhibit biofilm formation. Their efficacy depends on the size, dissolution into silver ions and stability of surface passivation [9, 23].

A diverse range of green synthesized AgNPs has been made and shown to inhibit the growth of pathogenic microbes via various mechanisms [24-28]. However, their fabrication reproducibility is hampered by their synthesis reactants' heterogeneity in composition and concentration. This translates to a lack of control over surface properties and size distribution. Consequently, varying results on their efficacy as antimicrobial substances are observed. Previous experiments have demonstrated that size-tuned and easily fuctionalizable AgNPs can be produced using citrate and tannic acid as reducing and stabilizing agents [29-32]. Moreover, commercial vendors offer citrate-stabilized AgNPs that can be used as a base for desirable biomolecule coating.

Betanin is then the main colouring molecule of red beetroot and has high antioxidant properties [33]. Beetroot extracts and purified betanin-synthesised AgNPs have been shown to possess antimicrobial activity [34-36]. Our recent studies detailed post-synthesis biomolecule functionalization of size-tuneable and easily surface-modifiable citrate-capped silver nanoparticles (CtAgNPs) with betanin and tested their antimicrobial activity [37]. Herein, we report the impact of the post-synthesis functionalized betanin silver nanoparticles (BtnAgNPs) on the cellular oxidative stress defence mechanism of *S. aureus* and biofilm-forming properties. This is in an effort to elucidate plausible routes through which BtnAgNPs inhibit the proliferation of *S. aureus*.

2. Materials and Methods

2.1. Materials

The following items were obtained from Himedia (Mumbai, India): tannic acid ($C_{76}H_{52}O_{46}$), silver nitrate ($AgNO_3$), sodium citrate tribasic dihydrate ($Na_3C_6H_5O_7.\ 2H_2O$), Mueller Hinton agar (MHA) and Mueller Hinton broth (MHB). Sigma-Aldrich (St. Louis, MO) provided betanin, 2', 7'-dichlorodihydrofluorescin diacetate (DCFH-DA), superoxide dismutase (SOD) and catalase assay kits. All solutions were made with ultrapure water (>18.2 MΩ.cm resistivity) prepared by PURELAB Option-Q™ (ELGA LabWater, UK). Teflon-coated stirrers and glassware used to prepare nanoparticles were first washed with a detergent, then aqua regia, thorough ultrapure water rinsing, and lastly with acetone.

2.2. Fabrication of post-synthesis functionalized betanin nanoparticles

The BtnAgNPs were prepared by ligand exchange functionalization of CtAgNPs of 37.9 ± 8.6 nm means size (transmission microscopy analysis) as per a previously reported procedure [37].

Briefly, to prepare the base CtAgNPs, 1 ml of $AgNO_3$ (25.00 mM) was quickly injected into 100 ml reflux boiling and continuously stirred solution containing $C_{76}H_{52}O_{46}$ and $Na_3C_6H_5O_7.\ 2H_2O$ at concentrations of 1 mM and 5.00 mM respectively. The mixture was transferred to a sterile glass media bottle and stored at 4 ℃ before purification. Excess

citrate and tannic acid were removed to yield purified nanoparticles. This was accomplished by first concentrating the particles through centrifuging the as-synthesized mix for 10 min at 10000 g in 1.5 ml centrifuge tubes utilizing an RC 4100™ centrifuge (Elteck, India). This was followed by the removal of the supernatant, adding 1.5 ml of 2.2 mM $Na_3C_6H_5O_7$. $2H_2O$ and shaking to suspend the particles. The centrifugation was done again, the supernatant removed, and the particles were re-suspended in 2.2 mM $Na_3C_6H_5O_7$. $2H_2O$ and stored under refrigeration.

2.3. Characterization of Nanoparticles

The formation of nanoparticles was monitored by obtaining an absorbance spectrum between 300-800 nm at 1nm intervals with a Model U-3900 double-beam spectrophotometer (Hitachi, Japan). A Nanotrac Wave™ model MN401 (Microtrac Inc., USA) was used to measure the hydrodynamic diameter and zeta potential. The equipment applied the dynamic light scattering (DLS) technique with the backscattering laser probe mounted at a 180 ° angle and set at 780 nm. The nanoparticles images, selected area diffraction (SAED) pattern and energy dispersive X-ray spectroscopy (EDS) spectrum were obtained using a JEM 2100F high resolution-transmission electron microscope (HR-TEM) at an acceleration voltage of 200 kV (Jeol, Japan). Transmission electron microscope image processing, size measurement and counting of nanoparticles were done using ImageJ 1.52n software [38]. The SAED gatan format diffraction patterns were analysed with the Get dSpace plug-in for ImageJ to determine and index the interplanar spacing. Computation of nanoparticles descriptive statistics and size distribution histogram was done with data analysis add-ins enabled Microsoft® Excel 2010. An Element™ XR spectrometer (Thermo Fisher Scientific, Germany), which applies high-resolution inductively coupled plasma mass spectrometry (HR-ICP-MS), was used to measure the total silver concentration in the purified nanoparticle colloids.

Characterization data was used to compute requisite information for functionalizing the nanoparticles. The mean surface area and nanoparticle count in the dispersions were estimated as outlined by Mbae and Umesha [37]. The mean volume of the nanoparticles was calculated using the mean diameter derived from TEM. Multiplication of volume with silver's density gave the average core mass. The number of nanoparticles/litre was estimated by dividing the total mass of silver in the solution computed from HR-ICP-MS calculations by the nanoparticles' average mass. A linear range UV-Vis absorbance calibration curve of silver concentration in the nanoparticle dispersion against absorbance at the maximum wavelength (λ_{max}) of the localized surface plasmon resonance (LSPR) was derived to quickly estimate nanoparticle concentration for use in bacterial growth media.

2.4. Post-synthesis functionalization with betanin

The procedure described by Mbae and Umesha [37] was used for the determination of the quantity of betanin to be added for nanoparticle ligand exchange. An assumption of 5 ligands per nm^2 was made and then an extra ×20 of what is required was provided to ensure adequate coverage and an excess amount. To produce BtnAgNPs, 1 ml aliquots of purified nanoparticle colloids at an estimated concentration of 3.3×10^{10} AgNPs/ml were put into 1.5 ml centrifuge tubes, 50 µl (0.5 mM) betanin aqueous solution added and the mixture was shaken for 12 h in darkness using a tube rocker. To remove excess betanin and displaced citrate, the colloid was subjected to centrifugation for 10 min at 10000 g and the supernatant was discarded. The pellet was cleaned by filling the tube with 1 ml of nano-pure water and repeating the centrifugation step. It was then re-dispersed in nano-pure water for characterization. Assessment of changes in the surface coating was done by measuring zeta potential and obtaining a UV-Vis spectrum.

2.5. Reactive Oxygen Species (ROS) quantification

The procedure described by Yuan *et al.* [14] was used to evaluate intracellular ROS. BtnAgNPs were added into *S. aureus* ATCC 12600 bacterial cells (10^6 CFU/ml) cultures to attain previously determined MIC of 12.5 ppm [37] and without (control) then incubated for 12 h at 37 ºC. The culture was then subjected to centrifugation at 300 g for 30 min in a cooled centrifuge (4 ºC). The supernatant was discarded and 100 µM of DCFH-DA was added to the wells and kept for 1 h. The fluorometric product in the sample was detected at λ_{ex}= 490 / λ_{em} = 520 nm and intensity used to indicate ROS levels.

2.6. Sample Preparation for Antioxidant Enzyme Activities

The lysate preparation for assessment of catalase and SOD activities was prepared as described by Martins *et al.* [39]. BtnAgNPs were added to give a final MIC concentration of 12.5 ppm in 10^6 CFU/ml, 500 µl cultures of *S. aureus* ATCC 12600 from the late exponential growth phase, then incubated for 24 h at 37°C. The supernatant was separated from the suspension by centrifugation at 3000 rpm for 5 min. After being rinsed twice with PBS, the pellet was resuspended in 500 µl of cell lysate buffer (1 mM EDTA, 10 mM Tris-HCl, 0.1% Triton-X-100, and 150 mM NaCl), then incubated for 1 h at 37°C. Cells were lysed by sonication followed by 5 min centrifugation at 3000 rpm and the supernatant was drawn for the tests.

2.7. Determination of Superoxide Dismutase

The previously outlined procedure by Tsamo *et al.* [40] employing the Sigma kit (catalogue no. MAK379) was followed for the assay. The water-soluble tetrazolium salt working solution (200 µl) and 20 µl each of the enzyme solution, and the cell lysate were combined. Absorbance was examined at 450 nm using an Infinite® 200Pro (Tecan, Switzerland) plate reader after incubation for 20 min at 37°C in the dark. The percentage inhibition was computed as the protocol. One Unit of enzyme activity corresponded to 50% inhibition. Bicinchoninic acid protein assay kit was used to determine lysate protein and SOD activity expressed as unit/mg protein.

2.8. Determination of Catalase Activity

Catalase assay kit (Sigma catalogue no. MAK381) was used to measure catalase activity according to the procedure outlined by Tsamo *et al.* [40]. In summary, 25 µl of 50 mM H_2O_2, 10 µl of cell lysate, and 750 µl of assay buffer (50 mM) were combined and incubated for 5 min. The reaction was then ended by adding 900 µl of stop solution (15 mM sodium azide) and vigorously mixing the contents. The reaction mixture was then divided into 10 µl portions put in separate tubes along with 1 ml of the colour reagent (2 mM 3,5-

dichloro-2-hydroxybenzenesulfonic acid and 0.25 mM 4-aminoantipyrine) before being incubated for 15 min. A plate reader model Infinite® 200Pro (Tecan, Switzerland) set at 520 nm was used to measure the absorbance and catalase activity computed in accordance with the protocol.

2.9. Impact of varying concentrations of BtnAgNPs on *S. aureus* biofilm forming ability

The broth microdilution technique was used for testing the effect of BtnAgNP on biofilm formation by *S. aureus* ATCC 12600. Briefly, columns 1 to 7 of 96 well-flat bottom plates were filled with 50 µl aliquots of sterile MHB. 100 µl nanoparticle colloid containing 50 ppm silver was added into column 8 wells. Column 1 was set aside for the BtnAgNPs-free negative control. Twofold serial dilutions of BtnAgNPs were performed between columns 2 and 7. A loop was used to obtain four typical colonies of *S. aureus* ATCC 12600 from an overnight MHA streak plate culture. The colonies were then homogenously distributed into 2 ml of MHB in a round-bottomed sterile culture tube using a vortex mixer. The optical density of the bacterial suspension was set to between 0.08 and 0.1 at 625 nm in disposable sterile plastic cuvettes. A 1:150 dilution was done to get about 1×10^6 CFU/ ml. The aliquots in column 1 and dilute BtnAgNPs in columns 2-7 wells were then mixed with 50 µl of the bacterial suspensions to provide a 5×10^5 CFU/ml cell count in 100 µl of the final portion. This gave a final test range of 0.4 to 12.5 ppm. The plates were wrapped in Parafilm® and kept at 37 °C for 24 h. The evaluation of the degree of biofilm inhibition was done according to Manukumar *et al*. [41]. Each well was washed with 200 µl sterile saline solution. Methanol (150 µl/well) was applied for 20 min to fix the biofilm. Plates were allowed to dry at ambient temperature for 30 min. The wells were stained with crystal violet (0.5% w/v) for 15 min, drained, and rinsed thrice using 200 µl of sterile saline water. The microplates were air-dried again at ambient temperature. Each well was treated with 95% ethanol (150 µl) for 30 min to remove the cell-bound dye. Absorbance was measured at 490 nm using an Infinite® 200Pro (Tecan, Switzerland) microplate reader for quantification. Biofilm inhibition trend was displayed by plotting the optical density against BtnAgNPs concentrations.

2.10. Statistics

The tests were repeated twice and performed in triplicates. Data analysis add-ins enabled Microsoft® Excel 2010 was used for statistical computations. Graphical presentations of means alongside standard deviation were done to demonstrate the trends. A two-tailed, paired sample *t*-test was used to compare the mean magnitudes of oxidative stress makers i.e. ROS, SOD and catalase in control and BtnAgNPs MIC treated samples. A *p*-value <0.05 was deemed statistically significant.

3. Results and Discussion

3.1. UV-Visible spectroscopy

The tendency of AgNPs colloidal solution to exhibit a LSPR peak makes UV-Vis spectroscopy an effective technique to monitor their evolution. The purified CtAgNPs exhibited an LSPR peak λ_{max} at 432 nm (Figure 1). Upon functionalization with betanin, the resulting BtnAgNPs displayed a slight LSPR λ_{max} peak red shift to 437 nm from 432 nm. This is a common observation results from dialectic constant change in the medium encircling the nanoparticle, providing a quick technique for monitoring a change in capping on CtAgNPs [42-44]. The BtnAgNPs spectrum did not show any second plasmon band at a higher wavelength, indicating no nanoparticle aggregation.

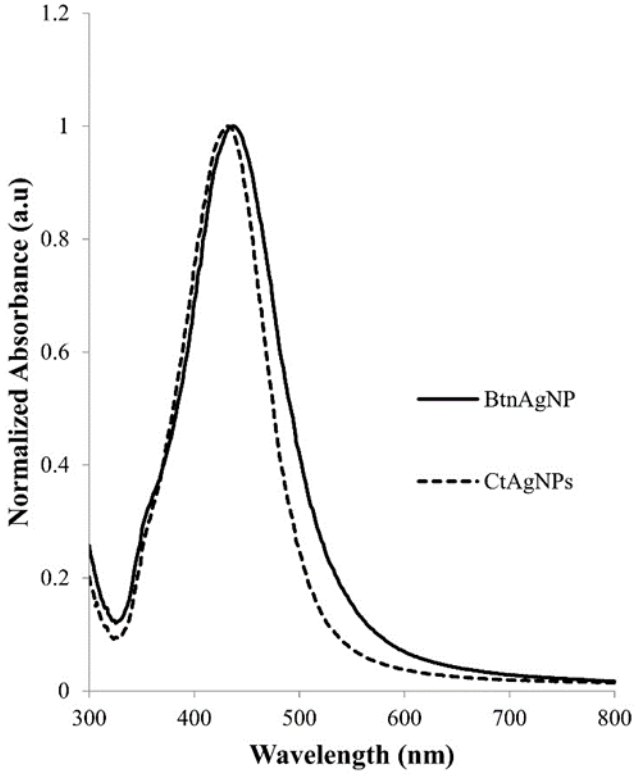

Fig 1: Absorption spectra of CtAgNPs (black dashed line) acquired before functionalization and BtnAgNPs (solid line) following ligand exchange with betanin

3.2. TEM, SAED, EDS, DLS and Zeta potential

Nanoparticle size and shape can be directly deciphered by TEM [45]. Subsequently, image analysis is used to compute size distribution. The particles had a mono-modal distribution and were roughly spherical with a TEM mean diameter of 37.9±8.6 nm (Figure 2(a)). Also shown in Figure 2(a) is the SAED image diffraction pattern analysis. The generated *d* space values of 2.365, 2.044, 1.457, and 1.225 Å were respectively indexed to (111), (200), (220), and (311) *hkl* lattice planes of face-centred cubic (fcc) structure of crystalline silver [46]. Additionally, EDS verified elemental silver presence (Figure 2(b). As shown in Figure 2(c), DLS analysis yielded a marginally bigger average diameter of 39.1 ±7.2 nm and a polydispersity index (PDI) of 0.6. When compared to TEM, DLS analysis has been noted to yield larger dimensions [47]. Nevertheless, both size determination techniques demonstrated a monomodal distribution. Employing $Na_3C_6H_5O_7$. $2H_2O$ and $C_{76}H_{52}O_{46}$ as reducing and stabilizing agents and strict adherence to synthesis protocol produces size- tuneable and loosely citrate electrostatic stabilized AgNPs that are easily functionalized [30, 45]. The ratio of reactants used was similar to the one applied by Bastús *et al*. [30]. They made CtAgNPs with a 36.9 ± 6.2 nm diameter, comparable to the 37.9 ± 8.6 nm achieved in this study. The CtAgNPs had a zeta potential of -32 mV, which was reduced to -28 mV upon capping change to yield BtnAgNPs. This served as a further confirmatory step for change in surface passivation and an indicator of the colloid stability. Dispersions are classified as moderately stable if their zeta potential is ± 20–30 mV [47]. Preferential displacement of citrate by betanin is hypothesized as the mechanism responsible for ligand exchange [37]. Betanin has all carboxyl groups deprotonated hence making it a tri-anion above neutral pH [33, 48]. There are two amine groups in betanin. Silver affinity for amine is higher than carboxyl groups [49, 50]. The amines were most likely oriented towards the nanoparticle surface, while the carboxyl groups conferred the overall negative charge on the shell.

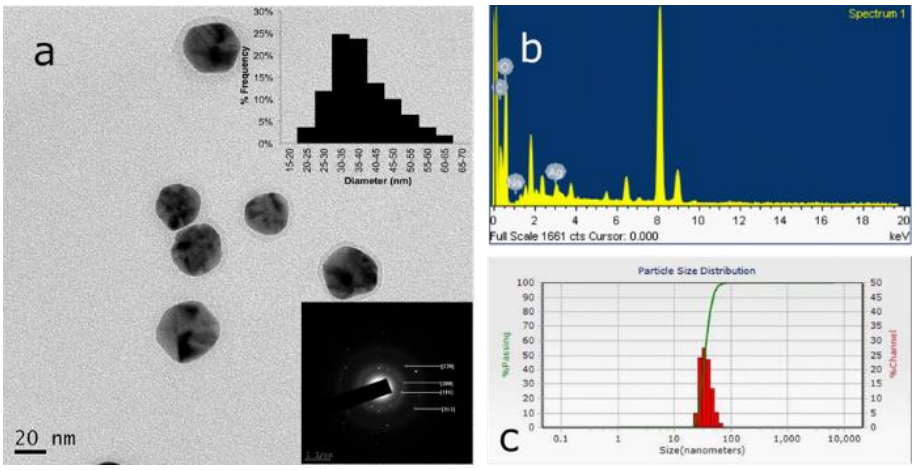

Fig 2: (a) Citrate-capped silver nanoparticles TEM photo. Inset: Top right-hand corner nanoparticles size distribution histogram (37.9 ± 8.6 nm average diameter) and bottom right-hand corner, SAED pattern depicting representative spots indexed to (111), (200), (220), and (311) *hkl* lattice planes of crystalline silver fcc structure (b) Ag peak at 3 keV on EDS spectrum (c) Size distribution bar graph of DLS analysis (average diameter 39.1 ± 7.2 nm) on a logarithmic x-axis, included is a solid line graph shows the passing cumulative per cent. PDI was 0.6.

3.3. Oxidative stress makers

The treatment of *S. aureus* with BtnAgNPs at 12.5 ppm increased the intracellular generation of ROS by 50% based on the comparative relative fluorescence intensity of the treated sample (577.0 ± 40.0) against the control (374.3 ± 27.3) (Figure 3). Exposure to BtnAgNPs led to reduced SOD production (26.1 ±3.3 U/mg) compared to the control (73.6 ± 5.3 U/mg) by *S. aureus* (Figure 4). Additionally, as shown in Figure 5, the catalase activity decreased from 11505.0 ± 231.8 U/mg to 2863.2 ±194.5 U/mg following a MIC BtnAgNPs treatment. Collectively the BtnAgNPs at the MIC significantly perturbed the redox physiological balance in *S. aureus* as part of their antimicrobial effects. The accumulation of ROS and depression of SOD and catalase production, important enzymes associated with oxidative stress attenuation in cellular systems demonstrate this. Similarly, Yuan *et al*. [14] observed an increase in ROS and down-regulation of both SOD and catalase in *S. aureus* isolates from mastitis-infected goats exposed to a MIC of quercetin synthesized AgNPs mean diameter of 20nm (size range 10-50 nm). Using fluorescence microscopy, biosynthesized AgNPs made using culture supernatants of corresponding test bacterial species were also demonstrated to increase the expression of ROS in *S. aureus* [51]. The immune system responds to infections with inflammation, followed by an oxidative burst leading to the production of ROS, which are bactericidal [52]. To counteract this oxidative attack, pathogenic bacteria such as *S. aureus* have developed an array of enzymatic and non-enzymatic antioxidant mechanisms [53]. Disabling these defences by antimicrobial agents leads to ROS's overwhelming of pathogen cells and death [10]. In addition to direct microbicidal activity, AgNPs have been shown to synergize the efficacy of antibiotics on pathogenic microbes [54].

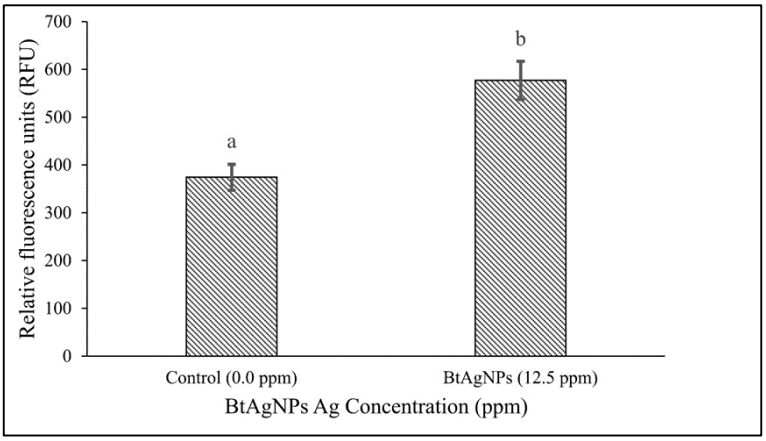

Fig 3: Effect of BtnAgNPs on ROS generation on *S. aureus* ATCC 12600. *S. aureus* cultures were incubated with a MIC of BtnAgNPs for 12 h. DCFH-DA was used to assess ROS generation. Results are means of tests conducted in triplicates and repeated twice. Standard deviation is shown by the error bars. Different letter labels denote statistically significant results ($p<0.05$)

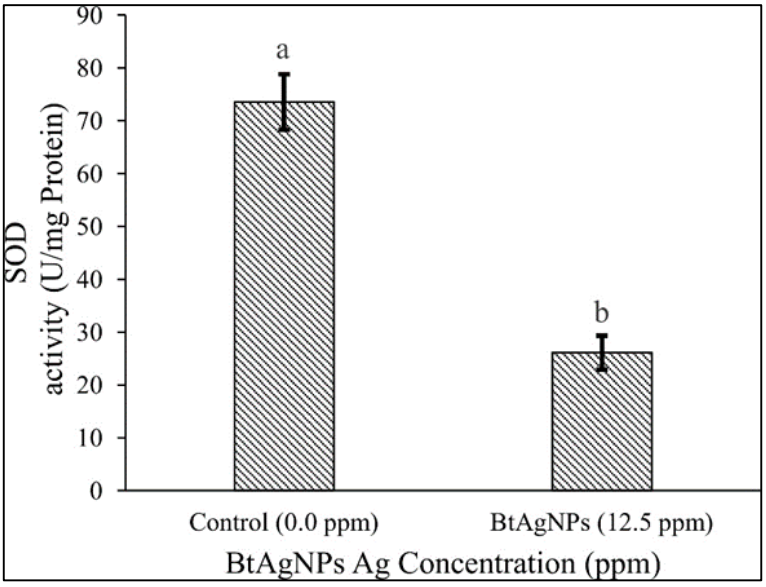

Fig 4: Effect of BtnAgNPs on SOD activity in *S. aureus* ATCC 12600. Bacterial cells were subjected to BtAgNPs MIC concentration for 24 h. Results are means of tests conducted in triplicates and repeated twice. Standard deviation is shown by the error bars. Different letter labels denote statistically significant results ($p<0.05$)

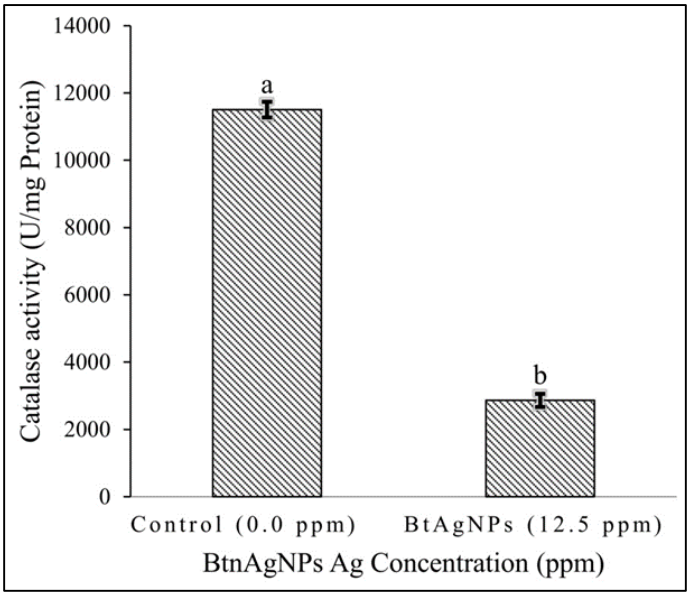

Fig 5: Effect of BtnAgNPs on catalase activity in *S. aureus* ATCC 12600. Bacterial cells were subjected to BtAgNPs MIC concentration for 24 h. Results are means of tests conducted in triplicates and repeated twice. Standard deviation is shown by the error bars. Different letter labels denote statistically significant results ($p<0.05$)

3.4. Anti-biofilm activity of the AgNPs

The SubMIC of BtnAgNPs decreased biofilm formation, as indicated in Figure 6. The highest level of inhibition corresponded with the MIC of 12.5 ppm. This translates to the nanoparticles' ability to disrupt this important virulent characteristic of *S. aureus*. Biofilm formation by *S. aureus* shields the pathogen from immune defence mechanisms and antimicrobial agents [55]. The concentration-dependent reduction in biofilm formation by BtnAgNPs observed in present studies has also been witnessed by other investigators using AgNPs of differing dimensions passivated by other biomolecules. AgNPs synthesized with beetroot extract whose betanin is the main betalain significantly reduced biofilm formation by clinical isolates of *S. aureus* [34]. Thymol-loaded chitosan silver nanoparticles 28.94 nm in size, were shown to reduce methicillin-resistant *S. aureus* 090 biofilm formation in a dose-based pattern [56]. Both *Zataria multiflora*-derived AgNPs and commercial AgNPs were observed to reduce biofilm formation, with the plant extract biosynthesized AgNPs demonstrating better inhibitory properties [23]. In addition to inducing ROS, biogenic AgNPs synthesized using *Desertifilum* sp. were also shown to inhibit biofilm formation in MRSA [57]. Silver nanoparticles of 28 nm average size synthesized using *Convolvulus arvensis* leaves extract inhibited biofilm formation with a minimum biofilm eradication concentration of 20 ppm against *S. aureus* [58]. At a pH of 9, *Foeniculum vulgare* seeds extract mediated AgNPs with a 49.62 nm hydrodynamic diameter and a MIC of 8 ppm against *S. aureus* (ATCC 25923) and several pathogenic isolates of *S. aureus*, inhibited biofilm formation at SubMICs in differing magnitudes based on strain type [28]. Other pathogenic bacteria have also witnessed biofilm formation attenuation by green synthesised AgNPs. *Penicillium chrysogenum*-derived AgNPs with a 48.2 nm mean hydrodynamic diameter exhibited strain-dependent biofilm inhibitory action against both *Acinetobacter baumannii* pathogenic isolates and *A. baumannii* (ATCC 19606) [59]. Varying the extract can have a differential impact on biofilm inhibition. For instance, *Lagerstroemia indica* extract synthesized AgNPs had higher biofilm inhibitory properties on *S. aureus* compared to *Alstonia scholaris* and *Aglaonema multifolium*-derived AgNPs [60]. Overall, the studies indicate the promising potential application of biomolecules stabilized AgNPs in controlling pathogenic bacteria.

The biological activity of metallic nanoparticles on different organisms is tied to the elemental nature of the nanoparticle, surface charge, size range, structure, and surface chemistry [2, 61]. This multiplicity effect was also demonstrated by size distribution variance, a higher expression of ROS, lethality and selectivity on cancerous cells by *Ocimum tenuiflorum* extract stabilized gold nanoparticles compared to citrate-capped gold nanoparticles [62].

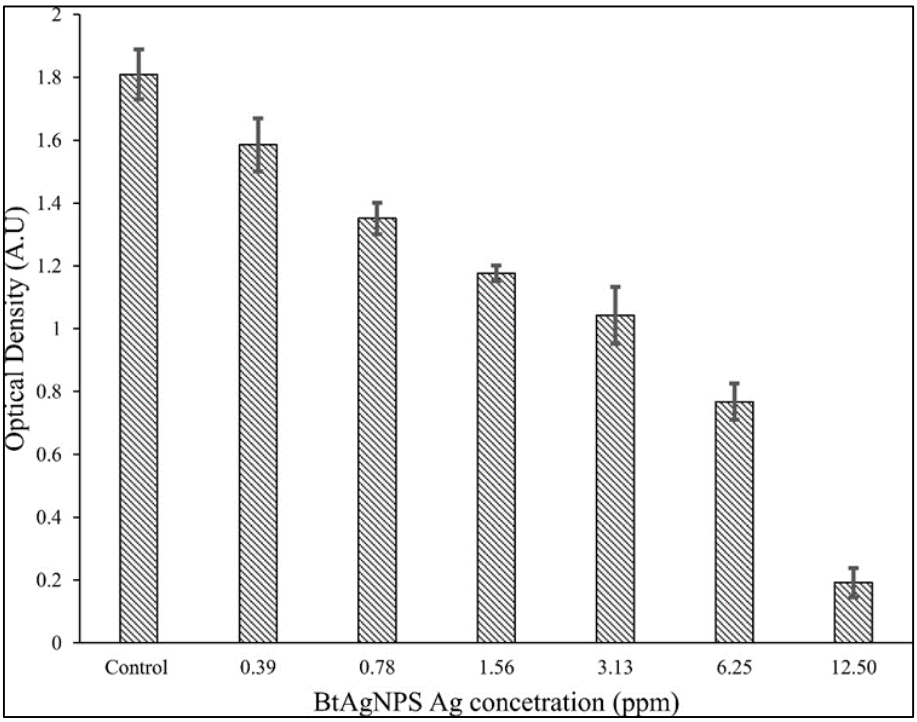

Fig 6: Reduction trend of bio-film formation by *S. aureus* ATCC 12600 upon exposure to SubMICs to MIC of BtnAgNPs. Values represent the mean absorbance (λ_{abs} =490nm) of the crystal violet-stained biofilms. Results are means of tests conducted in triplicates and repeated twice. The error bars indicate the standard deviation

4. Conclusion

AgNPs functionalized with biomolecules are an evolving tool that can provide alternative antimicrobial agents to fight pathogenic microbes. However, despite being ecologically friendly and very effective in controlling microbial growth, green synthesis systems yield AgNPs with a broad size range and complex surface capping, making comparative antimicrobial experiments challenging.

In this study, we introduced the aspect of post-synthesis functionalization of weakly passivated CtAgNP with betanin to yield BtnAgNPs. The MIC of BtnAgNPs was shown to upset the redox balance in standard *S. aureus* ATCC 12600 via accumulation of ROS and conversely reducing SOD and catalase activity. SubMICs of BtnAgNPs inhibited biofilm

formation in a concentration-dependent pattern. The findings support the perturbation of cellular antioxidant defence systems and disruption of biofilm formation as some of the key mechanisms that AgNPs target for bacteriostatic and bactericidal effects on *S. aureus*. Additionally, because it is well documented that variations in AgNP size, capping and synthesis techniques influence the overall efficacy of AgNPs, our results indicate it would be desirable to explore synthesis protocols that yield determinate sizes followed by appropriate biomolecule functionalization for easier cross-comparison of the effect of surface capping on antimicrobial properties.

5. Data Availability

Data associated with the study are incorporated in the manuscript. Further information can be availed by the corresponding author.

6. Conflicts of Interest

The authors declare that they have no conflicts of interest.

7. Funding Statement

Mbae, K.M. received support to follow PhD studies from the Scholarship Scheme for students from African countries through the Indian Council for Cultural Relations (ICCR), funded by the Ministry of External Affairs, Government of India

8. Acknowledgment

The authors are grateful to the sophisticated analytical instrument facility (SAIF) hosted by the Indian Institute of Technology, Mumbai, for providing HR-ICP-MS, HR-TEM, EDS and SAED facilities. Gratitude is also extended to the Institute of Excellence (IOE) housed by the University of Mysore for availing DLS and zeta potential analysis apparatus.

9. References

1. Rai M, Ingle AP, Gaikwad S, Gupta I, Gade A, Silvério da Silva S. Nanotechnology based anti-infectives to fight microbial intrusions. J Appl Microbiol 2016; 120(3):527-42.
2. Truong LB, Medina-Cruz D, Martínez-Sanmiguel JJ, Soto-Mendoza A, Esquivel-López IG, Pérez Y, *et al*. Chapter 8 - Biogenic metal nanomaterials to combat antimicrobial resistance [Internet]. In: Saravanan M, Barabadi H, Mostafavi E, Webster T, editors. Emerging Nanomaterials and Nano-Based Drug Delivery Approaches to Combat Antimicrobial Resistance. Elsevier; 2022 [cited 2023 Feb 15]. page 261-304. Available from: https://www.sciencedirect.com/science/article/pii/B9780323907927000117
3. Zakaria MY, Eraqi WA, Mohamed SA. Ultra-deformable free fatty acid based nano-carriers for topical delivery of Luteolin: A potential paradigm for management of Methicillin-Resistant Staphylococcus aureus skin infections. International Journal of Pharmaceutics 2023; 643:123259.
4. Dos Santos CA, Seckler MM, Ingle AP, Gupta I, Galdiero S, Galdiero M, *et al*. Silver Nanoparticles: Therapeutical Uses, Toxicity, and Safety Issues. Journal of Pharmaceutical Sciences. 2014; 103(7):1931-44.
5. Kim TH, Kim M, Park HS, Shin US, Gong MS, Kim HW. Size-dependent cellular toxicity of silver nanoparticles. J Biomed Mater Res. 2012; 100A (4):1033-43.
6. Ahlberg S, Rancan F, Epple M, Loza K, Höppe D, Lademann J, *et al*. Comparison of different methods to study effects of silver nanoparticles on the pro- and antioxidant status of human keratinocytes and fibroblasts. Methods. 2016; 109:55-63.
7. Sun D, Zhang W, Mou Z, Chen Y, Guo F, Yang E, *et al*. Transcriptome Analysis Reveals Silver Nanoparticle-Decorated Quercetin Antibacterial Molecular Mechanism. ACS Appl Mater Interfaces. 2017; 9(11):10047-60.
8. Beyth N, Houri-Haddad Y, Domb A, Khan W, Hazan R. Alternative Antimicrobial Approach: Nano-Antimicrobial Materials. Evidence-Based Complementary and Alternative Medicine. 2015; 2015:1-16.
9. Le Ouay B, Stellacci F. Antibacterial activity of silver nanoparticles: A surface science insight. Nano Today 2015; 10(3):339-54.
10. Gaupp R, Ledala N, Somerville GA. Staphylococcal response to oxidative stress. Front Cell Infect Microbiol [Internet] 2012 [cited 2020 Apr 22];2. Available from: https://www.frontiersin.org/articles/10.3389/fcimb.2012.00033/full
11. Majeed M, Hakeem KR, Rehman RU. Synergistic effect of plant extract coupled silver nanoparticles in various therapeutic applications- present insights and bottlenecks. Chemosphere. 2022; 288:132527.
12. Anthony KJP, Murugan M, Gurunathan S. Biosynthesis of silver nanoparticles from the culture supernatant of Bacillus marisflavi and their potential antibacterial activity. Journal of Industrial and Engineering Chemistry. 2014; 20(4):1505-10.
13. Han JW, Gurunathan S, Jeong JK, Choi YJ, Kwon DN, Park JK, *et al*. Oxidative stress mediated cytotoxicity of biologically synthesized silver nanoparticles in human lung epithelial adenocarcinoma cell line. Nanoscale Research Letters. 2014; 9(1):459.
14. Yuan YG, Peng QL, Gurunathan S. Effects of Silver Nanoparticles on Multiple Drug-Resistant Strains of Staphylococcus aureus and Pseudomonas aeruginosa from Mastitis-Infected Goats: An Alternative Approach for Antimicrobial Therapy. IJMS. 2017; 18(3):569.
15. Linz MS, Mattappallil A, Finkel D, Parker D. Clinical Impact of Staphylococcus aureus Skin and Soft Tissue Infections. Antibiotics. 2023; 12(3):557.
16. WHO. Antimicrobial resistance [Internet]. 2022 [cited 2022 Sep 25]; Available from: https://www.who.int/news-room/fact-sheets/detail/antimicrobial-resistance
17. Park JY, Seo KS. Staphylococcus aureus [Internet]. In: Food Microbiology. John Wiley & Sons, Ltd; 2019, [cited 2022 Sep 25]. page 555–84.Available from: https://onlinelibrary.wiley.com/doi/abs/10.1128/9781555819972.ch21
18. Narvaez-Bravo C, Toufeer M, Weese SJ, Diarra MS, Deckert AE, Reid-Smith R, *et al*. Prevalence of methicillin-resistant Staphylococcus aureus in Canadian commercial pork processing plants. Journal of Applied Microbiology. 2016; 120(3):770-80.
19. Petinaki E, Spiliopoulou I. Methicillin-resistant Staphylococcus aureus among companion and food-chain animals: impact of human contacts. Clinical Microbiology and Infection. 2012; 18(7):626-34.
20. Wendlandt S, Schwarz S, Silley P. Methicillin-Resistant

Staphylococcus aureus : A Food-Borne Pathogen? Annu Rev Food Sci Technol. 2013; 4(1):117-39.
21. Carfora V, Caprioli A, Marri N, Sagrafoli D, Boselli C, Giacinti G, *et al*. Enterotoxin genes, enterotoxin production, and methicillin resistance in Staphylococcus aureus isolated from milk and dairy products in Central Italy. International Dairy Journal. 2015; 42:12-5.
22. Parsek MR, Singh PK. Bacterial Biofilms: An Emerging Link to Disease Pathogenesis. Annual Review of Microbiology. 2003; 57(1):677-701.
23. Barabadi H, Mojab F, Vahidi H, Marashi B, Talank N, Hosseini O, *et al*. Green synthesis, characterization, antibacterial and biofilm inhibitory activity of silver nanoparticles compared to commercial silver nanoparticles. Inorganic Chemistry Communications. 2021; 129:108647.
24. Arshad H, Sami MA, Sadaf S, Hassan U. Salvadora persica mediated synthesis of silver nanoparticles and their antimicrobial efficacy. Sci Rep. 2021; 11(1):5996.
25. Arshad H, Sadaf S, Hassan U. De-novo fabrication of sunlight irradiated silver nanoparticles and their efficacy against E. coli and S. epidermidis. Sci Rep. 2022; 12(1):676.
26. Arshad H, Saleem M, Pasha U, Sadaf S. Synthesis of Aloe vera-conjugated silver nanoparticles for use against multidrug-resistant microorganisms. Electronic Journal of Biotechnology. 2022; 55:55-64.
27. Raghava S, Munene Mbae K, Umesha S. Green synthesis of silver nanoparticles by Rivina humilis leaf extract to tackle growth of Brucella species and other perilous pathogens. Saudi Journal of Biological Sciences. 2021; 28(1):495-503.
28. Talank N, Morad H, Barabadi H, Mojab F, Amidi S, Kobarfard F, *et al*. Bioengineering of green-synthesized silver nanoparticles: In vitro physicochemical, antibacterial, biofilm inhibitory, anticoagulant, and antioxidant performance. Talanta. 2022; 243:123374.
29. Dadosh T. Synthesis of uniform silver nanoparticles with a controllable size. Mater Lett. 2009; 63(26):2236-8.
30. Bastús NG, Merkoçi F, Piella J, Puntes V. Synthesis of Highly Monodisperse Citrate-Stabilized Silver Nanoparticles of up to 200 nm: Kinetic Control and Catalytic Properties. Chem Mater. 2014; 26(9):2836-46.
31. Rainville, *et al*. 2013 Controlled synthesis of low polydispersity Ag@SiO2.pdf.
32. Ranoszek-Soliwoda K, Tomaszewska E, Socha E, Krzyczmonik P, Ignaczak A, Orlowski P, *et al*. The role of tannic acid and sodium citrate in the synthesis of silver nanoparticles. J Nanopart Res. 2017; 19(8):273.
33. Gliszczyńska-Świgło A, Szymusiak H, Malinowska P. Betanin, the main pigment of red beet: Molecular origin of its exceptionally high free radical-scavenging activity. Food Addit Contam. 2006; 23(11):1079-87.
34. Vijaya D, Raj NT. Antibacterial and Antibiofilm Activity of Silver Nanoparticles Synthesised by Beetroot Containing Betalains Pigment on Clinical Bacterial Isolates. JCDR [Internet] 2022 [cited 2023 Sep 3]; Available from: https://www.jcdr.net//article_fulltext.asp?issn=0973-709x&year=2022&month=September&volume=16&issue=9&page=FC01-FC06&id=16830
35. Bindhu MR, Umadevi M. Antibacterial and catalytic activities of green synthesized silver nanoparticles. Spectrochimica Acta Part A: Molecular and Biomolecular Spectroscopy. 2015; 135:373-8.
36. Kosa SA, Zaheer Z. Betanin assisted synthesis of betanin@silver nanoparticles and their enhanced adsorption and biological activities. Food Chemistry. 2019; 298:125014.
37. Mbae KM, Umesha S. Physicochemical and antimicrobial properties of post-synthesis betanin and chitosan oligosaccharide functionalized silver nanoparticles. J Nanopart Res. 2020; 22(11):346.
38. Schneider CA, Rasband WS, Eliceiri KW. NIH Image to ImageJ: 25 years of image analysis. Nat Methods 2012; 9:671-5.
39. Martins D, McKay G, Sampathkumar G, Khakimova M, English AM, Nguyen D. Superoxide dismutase activity confers (p)ppGpp-mediated antibiotic tolerance to stationary-phase Pseudomonas aeruginosa. Proceedings of the National Academy of Sciences. 2018; 115(39):9797-802.
40. Tsamo DLF, Tamokou JDD, Kengne IC, Ngnokam CDJ, Djamalladine MD, Voutquenne-Nazabadioko L, *et al*. Antimicrobial and Antioxidant Secondary Metabolites from Trifolium baccarinii Chiov. (Fabaceae) and Their Mechanisms of Antibacterial Action. BioMed Research International. 2021; 2021:e3099428.
41. Manukumar HM, Chandrasekhar B, Rakesh KP, Ananda AP, Nandhini M, Lalitha P, *et al*. Novel T-C@AgNPs mediated biocidal mechanism against biofilm associated methicillin-resistant Staphylococcus aureus (Bap-MRSA) 090, cytotoxicity and its molecular docking studies. Med Chem Commun. 2017; 8(12):2181-94.
42. Barbalinardo M, Caicci F, Cavallini M, Gentili D. Protein Corona Mediated Uptake and Cytotoxicity of Silver Nanoparticles in Mouse Embryonic Fibroblast. Small. 2018; 14(34):1801219.
43. Bastús NG, Piella J, Puntes V. Quantifying the Sensitivity of Multipolar (Dipolar, Quadrupolar, and Octapolar) Surface Plasmon Resonances in Silver Nanoparticles: The Effect of Size, Composition, and Surface Coating. Langmuir 2016; 32(1):290-300.
44. Shen H, Lu G, Zhang T, Liu J, Gu Y, Perriat P, *et al*. Shape effect on a single-nanoparticle-based plasmonic nanosensor. Nanotechnology. 2013; 24(28):285502.
45. Hühn J, Carrillo-Carrion C, Soliman MG, Pfeiffer C, Valdeperez D, Masood A, *et al*. Selected Standard Protocols for the Synthesis, Phase Transfer, and Characterization of Inorganic Colloidal Nanoparticles. Chem Mater. 2017; 29(1):399-461.
46. Edington JW. Electron Diffraction in the Electron Microscope [Internet]. In: Edington JW, editor. Electron Diffraction in the Electron Microscope. London: Macmillan Education UK; 1975 [cited 2019 Jul 23]. page 1–77.Available from: https://doi.org/10.1007/978-1-349-02595-4_1
47. Bhattacharjee S. DLS and zeta potential – What they are and what they are not? J Control Release 2016; 235:337-51.
48. Frank T, Stintzing FC, Carle R, Bitsch I, Quaas D, Straß G, *et al*. Urinary pharmacokinetics of betalains following consumption of red beet juice in healthy humans. Pharmacol Res. 2005; 52(4):290-7.
49. Baalousha M, Afshinnia K, Guo L. Natural organic matter composition determines the molecular nature of silver nanomaterial-NOM corona. Environ Sci Nano. 2018; 5(4):868-81.

50. Bell RA, Kramer JR. Structural chemistry and geochemistry of silver-sulfur compounds: Critical review. Environ Toxicol Chem. 1999; 18(1):9-22.
51. Quinteros MA, Cano Aristizábal V, Dalmasso PR, Paraje MG, Páez PL. Oxidative stress generation of silver nanoparticles in three bacterial genera and its relationship with the antimicrobial activity. Toxicology in Vitro. 2016; 36:216-23.
52. Bishayi B, Bandyopadhyay D, Majhi A, Adhikary R. Possible Role of Toll-like Receptor-2 in the Intracellular Survival of Staphylococcus aureus in Murine Peritoneal Macrophages: Involvement of Cytokines and Anti-Oxidant Enzymes. Scandinavian Journal of Immunology. 2014; 80(2):127-43.
53. Grunenwald CM, Choby JE, Juttukonda LJ, Beavers WN, Weiss A, Torres VJ, *et al*. Manganese Detoxification by MntE Is Critical for Resistance to Oxidative Stress and Virulence of Staphylococcus aureus. mBio. 2019; 10(1):e02915-18.
54. Wan G, Ruan L, Yin Y, Yang T, Ge M, Cheng X. Effects of silver nanoparticles in combination with antibiotics on the resistant bacteria Acinetobacter baumannii. IJN 2016; 11:3789-800.
55. Goswami SR, Sahareen T, Singh M, Kumar S. Role of biogenic silver nanoparticles in disruption of cell–cell adhesion in Staphylococcus aureus and Escherichia coli biofilm. Journal of Industrial and Engineering Chemistry. 2015; 26:73-80.
56. Manukumar HM, Yashwanth B, Umesha S, Venkateswara Rao J. Biocidal mechanism of green synthesized thyme loaded silver nanoparticles (GTAgNPs) against immune evading tricky methicillin-resistant Staphylococcus aureus 090 (MRSA090) at a homeostatic environment. Arab J Chem. 2017; S1878535217301880.
57. Hamida RS, Ali MA, Goda DA, Khalil MI, Al-Zaban MI. Novel Biogenic Silver Nanoparticle-Induced Reactive Oxygen Species Inhibit the Biofilm Formation and Virulence Activities of Methicillin-Resistant Staphylococcus aureus (MRSA) Strain. Front Bioeng Biotechnol [Internet] 2020 [cited 2021 May 5]; 8. Available from: https://www.frontiersin.org/articles/10.3389/fbioe.2020.00433/full
58. Hamedi S, Shojaosadati SA, Mohammadi A. Evaluation of the catalytic, antibacterial and anti-biofilm activities of the Convolvulus arvensis extract functionalized silver nanoparticles. Journal of Photochemistry and Photobiology B: Biology. 2017; 167:36-44.
59. Barabadi H, Mohammadzadeh A, Vahidi H, Rashedi M, Saravanan M, Talank N, *et al*. Penicillium chrysogenum-Derived Silver Nanoparticles: Exploration of Their Antibacterial and Biofilm Inhibitory Activity Against the Standard and Pathogenic Acinetobacter baumannii Compared to Tetracycline. J Clust Sci. 2022; 33(5):1929-42.
60. Hosnedlova B, Kabanov D, Kepinska M, B Narayanan VH, Parikesit AA, Fernandez C, *et al*. Effect of Biosynthesized Silver Nanoparticles on Bacterial Biofilm Changes in S. aureus and E. coli. Nanomaterials. 2022; 12(13):2183.
61. Barabadi H, Vahidi H, Mahjoub MA, Kosar Z, Damavandi Kamali K, Ponmurugan K, *et al*. Emerging Antineoplastic Gold Nanomaterials for Cervical Cancer Therapeutics: A Systematic Review. J Clust Sci. 2020; 31(6):1173-84.
62. Virmani I, Sasi C, Priyadarshini E, Kumar R, Sharma SK, Singh GP, *et al*. Comparative Anticancer Potential of Biologically and Chemically Synthesized Gold Nanoparticles. J Clust Sci. 2020; 31(4):867-76.